Topics in Catalysis (2018) 61:530–541
https://doi.org/10.1007/s11244-018-0907-4

ORIGINAL PAPER

The Methanol Economy: Methane and Carbon Dioxide Conversion

Wen-Chi Liu[1,2] · Jayeon Baek[3] · Gabor A. Somorjai[1,2]

Published online: 8 March 2018

Abstract
Need for clean energy is imminent and methanol is considered as a promising alternative energy source. Conventional process for the production of methanol has been achieved via syngas which is derived by the steam reforming of methane or naphtha and the gasification of coal. Methanol can also be prepared by direct oxidation of methane (natural gas) or reduction of carbon dioxide (CO_2) with hydrogen. In this way, carbon-neutral cycling can be achieved and world's dependence on fossil fuels will be alleviated. In this minireview, we will address case by case some recent advancements in the conversion of methane and CO_2 to methanol both homogeneously and heterogeneously with emphasis on the contribution from Professor George A. Olah's and our group. In the end, a short outlook is provided towards existing problems and future opportunities.

Keywords Methanol economy · CO_2 hydrogenation · Direct methane to methanol (DMTM) process · Bi-reforming of methane

1 Introduction

This paper is dedicated to the memory of Professor George A. Olah who was a pioneer for methanol economy. In his iconic paper "Beyond oil and gas: The methanol economy" [1], Olah argued that the methanol economy can replace fossil fuels. Methanol can be used as a convenient energy storage material, a fuel, and a feedstock to synthesize hydrocarbons which mankind get from fossil fuel nowadays [2, 3]. It is also proposed that methanol can be produced from the reduction of recycled CO_2, a major source of global warming, which merits from its renewability and methane (natural gas), which is abundant and will last well into the next century.

One of the importance of methanol comes from its direct use as a fuel or blending with gasoline to improve the octane number although it has half the volumetric energy density (15.6 MJ/L) relative to gasoline (34.2 MJ/L) and diesel (38.6 MJ/L) [4–6]. There had been 15,000 methanol-powered cars during the 1990s granted by Environmental Protection Agency (EPA), but the use was discontinued due to an increased natural gas price [7]. Recently, there are some pilot projects to restart the methanol-powered cars operating with the renewable methanol produced from recycled CO_2 in Europe and China by CRI and Geely. Methanol can also be used to generate electricity by direct methanol fuel cell (DMFC) at ambient temperature, where methanol is oxidized into CO_2 at the anode and oxygen is reduced at the cathode to produce water [8–12].

Methanol is also a key feedstock for chemical manufacturing. The most major derivatives from methanol are formaldehyde, acetic acid, methyl tertiary butyl ether (MTBE), and dimethyl ether (DME). In recent years, methanol-to-hydrocarbons (MTH) research has been growing rapidly including methanol-to-gasoline (MTG) and methanol-to-olefins (MTO) technology [13–15], where the selectivity to different classes of hydrocarbons is found to be determined by zeolite topology and operating conditions.

Methanol is commonly produced from syngas containing 2–8 vol% of CO_2 in a $CO/CO_2/H_2$ stream [16]. Syngas is mostly obtained from steam reforming of methane (Eqs. 1

Wen-Chi Liu and Jayeon Baek have contributed equally to the work.

✉ Gabor A. Somorjai
somorjai@berkeley.edu

[1] Department of Chemistry, Kavli Energy Nanosciences Institute, University of California, Berkeley, Berkeley, CA 94720, USA

[2] Chemical Sciences Division, Lawrence Berkeley National Laboratory, Berkeley, CA 94720, USA

[3] Department of Chemical & Biomolecular Engineering, University of California, Berkeley, Berkeley, CA 94720, USA

and 2) followed by steam reforming of naphtha and gasification of coal [17]. The ratio of $CO/CO_2/H_2$ in the feed is often varied depending on the source. Today, CO_2 is added up to 30% of the total carbon in syngas [18] and the H_2 concentration in the feed is compensated by the water–gas shift reaction (WGS) according to Eq. 5. The addition of CO_2 in syngas improves the methanol yield as the rate of hydrogenation of CO_2 (Eq. 3) is much greater than that of CO (Eq. 4) [19, 20].

$$\text{Steam reforming} \quad CH_4 + H_2O \rightarrow CO + 3H_2 \quad \Delta H_{298\,K} = +49.3 \text{ kcal/mol} \tag{1}$$

$$\text{Steam reforming} \quad CH_4 + 2H_2O \rightarrow CO_2 + 4H_2 \quad \Delta H_{298\,K} = +39.3 \text{ kcal/mol} \tag{2}$$

$$\text{Methanol synthesis} \quad CO_2 + 3H_2 \rightarrow CH_3OH + H_2O \quad \Delta H_{298\,K} = -11.8 \text{ kcal/mol} \tag{3}$$

$$\text{Methanol synthesis} \quad CO + 2H_2 \rightarrow CH_3OH \quad \Delta H_{298\,K} = -21.6 \text{ kcal/mol} \tag{4}$$

$$\text{Water-gas shift reaction} \quad CO + H_2O \rightarrow CO_2 + H_2 \quad \Delta H_{298\,K} = -9.8 \text{ kcal/mol} \tag{5}$$

Chinchen et al. conducted isotope experiment to determine the carbon source in methanol through the addition of ^{14}CO and $^{14}CO_2$ traces to $CO/CO_2/H_2$ reactant mixtures. Interestingly, it is found that in the range of P_{CO_2}/P_{CO} ratios from 0.02 to 1, around 70–100% of the methanol is made from CO_2 at 250 °C and 50 bar [21]. This result drove researchers to study CO_2 hydrogenation for both academic and environmental reasons.

Fascinated by the attractive concept of combining carbon capture and storage (CSS) and hydrogenation of CO_2 to methanol, there have been significant developments in this field. However, most of the works are devoted to uncovering the correlation between the synthesis and activity in Cu/ZnO or Cu/ZrO_2 based catalysts [22–28]. Recently, we developed new types of heterogeneous catalysts with high activity and selectivity in converting CO_2 to methanol.

On the other hand, direct methane to methanol (DMTM) process has emerged as one of the 'Holy Grails of catalysis', but the chemical inertness of the C–H bond in methane and the instability of methane oxygenates render it impractical [29–31]. Despite these difficulties, there are a number of heterogeneous catalysts discovered which are capable of activating methane at low temperature for the production of methanol [32–34].

In this minireview, we will introduce some of our recent developed heterogeneous catalysts for methanol production from CO_2 as well as Professor George Olah's work on the homogeneous CO_2 hydrogenation to methanol. In later sections, the evolved heterogeneous catalysts and their active sites for DMTM will be described, following which the bi-reforming process developed by Professor George Olah for the efficient production of 'metgas' will also be discussed. After a brief summary of the current knowledge, a short outlook is given on the existing problems and possible opportunities.

2 Catalytic Conversion of CO_2 and Methane to Methanol

2.1 The George Olah Plant

The first commercialized plant using CO_2 and hydrogen to produce methanol was inaugurated in 2012 in Iceland by Carbon Recycling International (CRI). The plant was named in honor of Professor George A. Olah. The George Olah plant uses captured CO_2 from flue gas originated from geothermal steam emissions and H_2 generated by water splitting where electrolysis operates with geothermal electricity. The produced methanol is called Vulcanol™ as the energy comes from Volcano. In the overall reaction, there is no toxic byproduct generated and it gives O_2 from water splitting (Fig. 1). CRI currently uses Cu and ZnO based solid catalyst for the hydrogenation of CO_2, which is the conventional catalyst for the production of methanol from syngas [35].

2.2 Catalytic Conversion of CO_2 to Methanol

2.2.1 Hybrid Oxide Catalyst: MnO_x Nanoparticles (NPs) Supported on Mesoporous Co_3O_4 (m-Co_3O_4)

Despite the classic $Cu/ZnO/Al_2O_3$ catalyst, novel hybrid-oxide systems, such as $MnO_x/m\text{-}Co_3O_4$ [37], In_2O_3/ZrO_2 [38], and $ZnO–ZrO_2$ [39] have been developed and shown to exhibit promising performance in the conversion of CO_2 to methanol, which provides potential alternatives towards higher efficiency both catalytically and economically. Synergistic effect existing between the interfaces of the two components was proven to be crucial in delivering the high performance over these catalysts [40, 41].

Specifically, the $MnO_x/m\text{-}Co_3O_4$ catalyst was developed in our group for the production of methanol under mild reaction conditions. The catalyst consists of colloidally synthesized 6 nm manganese oxide NPs supported on a mesoporous cobalt oxide support (Fig. 2a, b), which was fabricated via a hard-templating method with mesoporous silica KIT-6 [42]. High-angle annual dark-field (HAADF) images and energy-dispersive X-ray spectroscopy (EDS) elemental mapping results indicate a homogeneous distribution of the supported MnO_x NPs (Fig. 2c–e). Catalytic

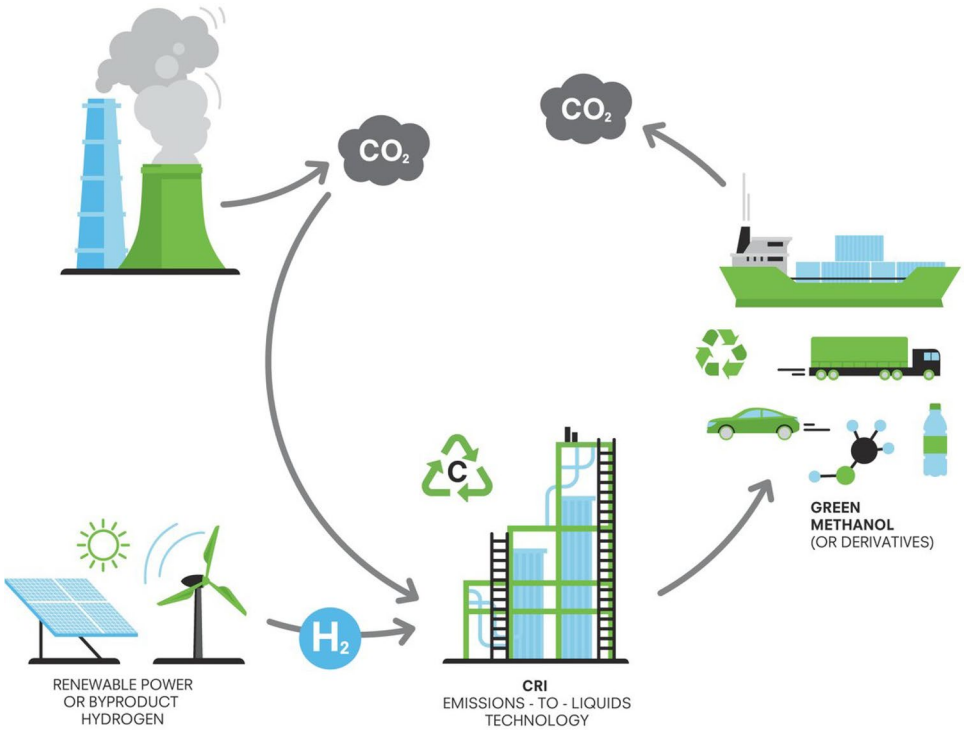

Fig. 1 Flowchart of Carbon Recycling International's (CRI) Emission to Liquids (EtL) process [36]

evaluation in the hydrogenation of CO_2 revealed high selectivity towards methanol (up to 30%) with a turnover frequency of $> 0.8\ s^{-1}$ at 250 °C and 6 bar. As compared to the commercial $Cu/ZnO/Al_2O_3$ methanol catalyst, not only the hybrid catalyst shows much higher methanol yield ($0.18\ s^{-1}$ vs. 0.01–0.02 s^{-1}), but it also operates at much milder conditions (1–6 bar vs. 10–50 atm), which makes it more energy-efficient and cost-effective.

The origin of the outstanding performance was attributed to the presence of an active interface between cobalt oxide surface layers and MnO_x NPs, as revealed by various characterization techniques, including X-ray absorption spectroscopy (XAS) and electron energy-loss spectroscopy (EELS), together with reactor study of carefully designed control experiments.

As compared to the fresh catalyst, the used one shows a more reduced nature of Co, as suggested by the decreased ratio of O to Co from 1.4 to 0.3 obtained by EELS measurements. Surface sensitive XAS analysis further confirmed the surface in favor of Co(II) oxide, indicating a core/shell structure with a metallic core and a Co(II) oxide shell. The role of different components within the hybrid catalyst was illustrated by running the reaction with each alone and with an inverted catalyst fabricated by depositing CoO_x NPs on m-MnO_2. Catalysts with MnO_x NPs alone mainly produced CO with low TOF, while m-Co_3O_4 by itself showed moderate activity with selectivity towards CO, CH_4, and methanol (Fig. 2f). It was suggested that the MnO_x first reduces CO_2 to form CO, which would then migrate to the interface area and produce methanol. This idea was further proven by testing the inverted catalyst, of which the performance closely resembles that of MnO_x alone.

2.2.2 Metal–Organic Framework (MOF) as a Promoting Co-catalyst: Cu Nanocrystal Encapsulated in UiO-66

Selective production of methanol from CO_2 is somewhat challenging because it gives other side products. CO is a main side product over $Cu/ZnO/Al_2O_3$ as a result of reverse WGS reaction ($CO_2 + H_2 \rightleftharpoons CO + H_2O$) [43]. To address this issue, we developed a novel catalyst consisting of a single Cu nanocrystal encapsulated within a single Zr(IV)-based MOF denoted as Cu⊂UiO-66 [UiO-66 = $Zr_6O_4(OH)_4(BDC)_6$, BDC = 1,4-benzenedicarboxylate] as shown in Fig. 3a. The catalytic activity of Cu⊂UiO-66 was compared with $Cu/ZnO/Al_2O_3$ in the temperature range of 175–250 °C (Fig. 3b). Notably, Cu⊂UiO-66 catalyst gives a eightfold enhancement in TOF as compared to the benchmark $Cu/ZnO/Al_2O_3$ catalyst and 100% selectivity to methanol in the CO_2 hydrogenation reaction at 200 °C and 10 bar [44]. As the reverse WGS reaction is endothermic ($\Delta H_{298\ K} = 9.8$ kcal/mol) whereas the hydrogenation of CO_2 is exothermic ($\Delta H_{298\ K} = -11.8$ kcal/mol), CO production is expected to increase as the reaction temperature increases, which is the case for the $Cu/ZnO/Al_2O_3$ catalyst. However, interestingly, Cu⊂UiO-66 gives only methanol as the product across the temperature range tested.

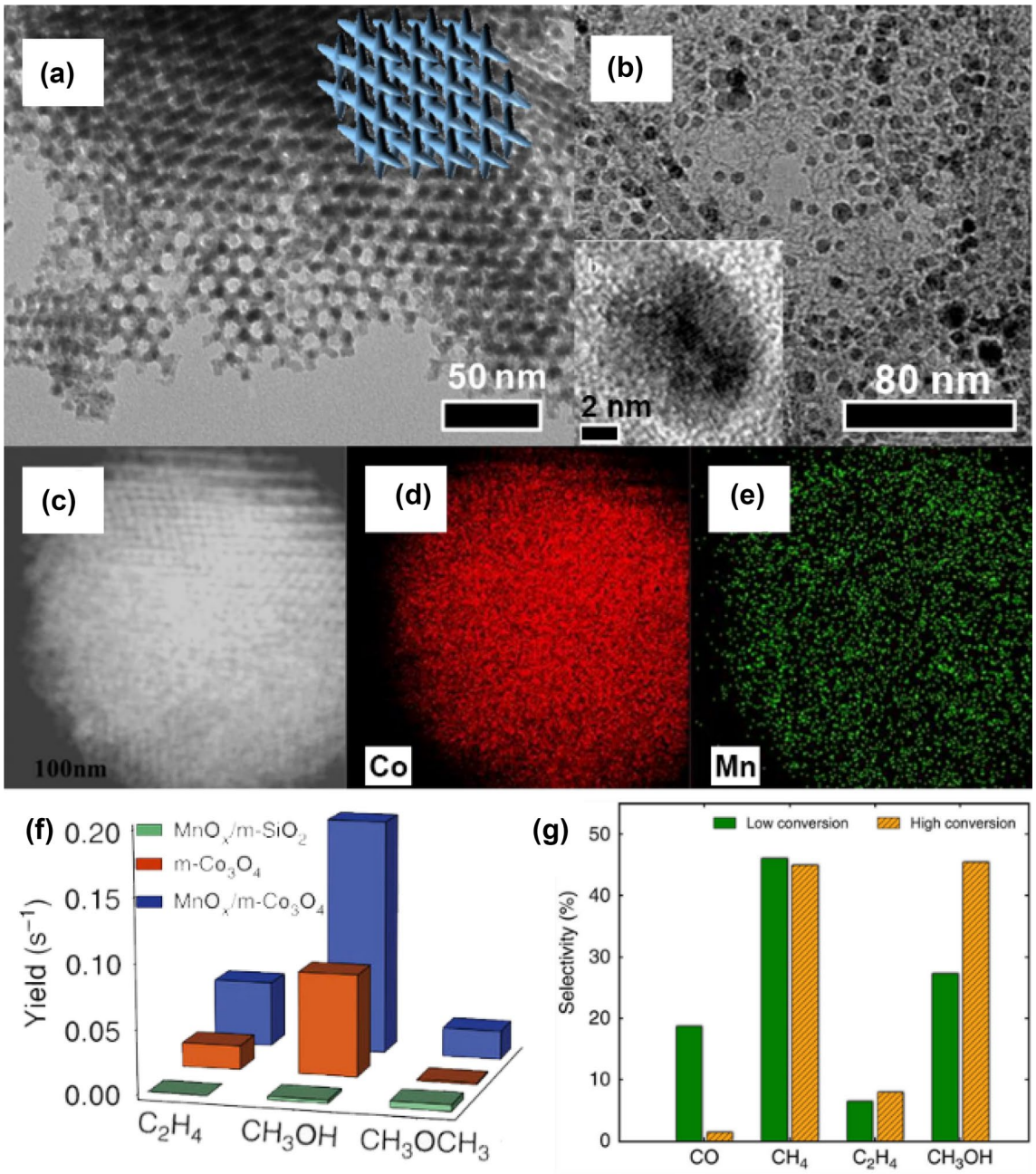

Fig. 2 TEM images of **a** m-Co_3O_4 and **b** 6 nm MnO NPs. **c** HAADF image and EDS elemental mapping results of **d** Co and **e** Mn of the hybrid MnO_x/m-Co_3O_4 catalyst. **f** Reaction yields on m-Co_3O_4, MnO_x/m-SiO_2, and MnO_x/m-Co_3O_4 catalysts. **g** Product distribution at low and high reaction conversions. **a** Adapted with permission from reference [42]. Copyright 2013 American Chemical Society; **b**–**g** adapted with permission from reference [37]. Copyright 2015 Springer Nature

The excellent performance of the Cu⊂UiO-66 catalyst can be attributed to the strong metal-support interaction (SMSI) effect confirmed by X-ray photoelectron spectroscopy (XPS) analysis (Fig. 3c). Here, we selected Cu nanocrystal supported on UiO-66 as a proxy for Cu⊂UiO-66 as the distance between the embedded Cu nanocrystal and the Cu⊂UiO-66 surface is beyond the escape depth of the photoelectrons in the XPS measurement. In UiO-66 without Cu nanocrystals, Zr $3d_{5/2}$ at 182.8 eV represents Zr(IV) in the Zr oxide secondary building unit [SBU:$Zr_6O_4(OH)_4(BDC)_6$] [45]. We observed that Zr $3d_{5/2}$ is shifted to 182.2 eV after the addition of Cu nanocrystals, which indicates a reduction of Zr(IV) and implies a SMSI effect between Cu nanocrystals and UiO-66. Correspondingly, there is an oxidation of Cu nanocrystals at the interface, where mixed states of metallic and cationic Cu species are formed. This promotes methanol

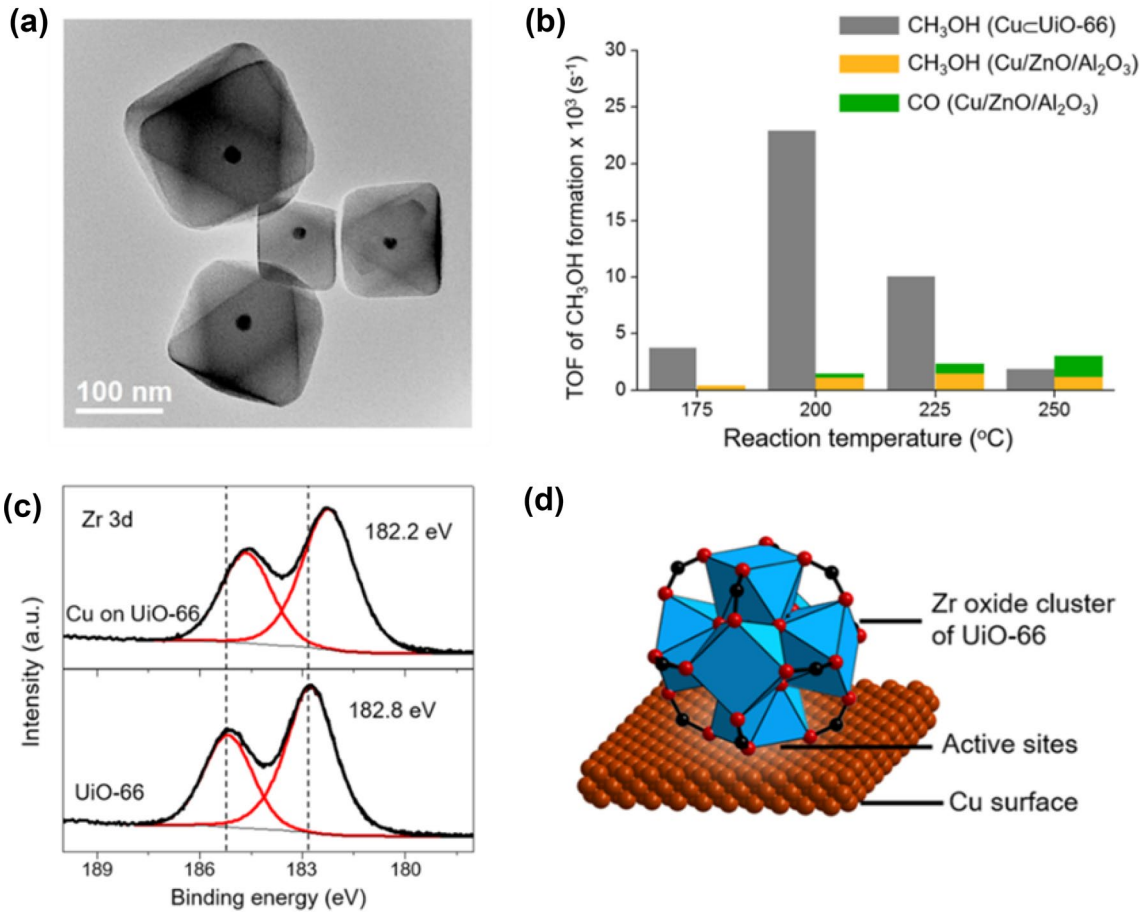

Fig. 3 **a** TEM image of Cu⊂UiO-66 catalyst. **b** TOFs of product formation over Cu⊂UiO-66 and $Cu/ZnO/Al_2O_3$ catalysts at various reaction temperatures. **c** XPS spectra of Zr 3d level of UiO-66 and Cu on UiO-66. **d** Illustration of the active site of the Cu⊂UiO-66 catalyst. One Zr oxide SBU $[Zr_6O_4(OH)_4(–CO_2)_{12}]$ is used as a representative of ordered array of SBUs. Atom labeling scheme: Cu, brown; C, black; O, red; Zr, blue polyhedra. H atoms are omitted for clarity. Adapted with permission from reference [44]. Copyright 2016 American Chemical Society

production by (i) dissociation of H_2 on the metallic Cu and (ii) stabilization of the intermediates (i.e., formate) by cationic Cu species, as the rate determining step in this reaction is the hydrogenation of surface formate, which can be accelerated by the adsorbed hydrogen in its vicinity. Thus, the active sites of this reaction locate at the interface between Cu nanocrystal and Zr oxide cluster $[Zr_6O_4(OH)_4(BDC)_6]$ as described in Fig. 3d. This is the first report that shows SMSI effect between the metal nanocrystal and metal–organic framework.

2.2.3 The Homogeneous Approach: Single Molecularly Defined Catalysts

In contrast to the well-developed heterogeneous route that has been already commercialized, CO_2 hydrogenation to methanol via homogeneous approach remained relatively unexplored until not too long ago [46–49]. As compared to its heterogeneous counterpart, converting CO_2 to methanol using homogeneous catalysts owns its advantages in many folds. First of all, reaction selectivity seen with homogeneous catalysts is exceptional, with numbers as close to 100% being reported. In addition, the reaction is often carried out at milder conditions, making the whole process more energy efficient. Furthermore, catalyst activity could be tuned both by changing the metal site and tailoring the ligand environment, allowing for rational design and systematic optimization of the catalyst system.

Ever since the pioneering work by Milstein and coworkers on the hydrogenation of organic carbonates and formates to alcohols [50], novel catalyst systems have been continuously developed which enable the catalytic conversion of CO_2 to methanol with outstanding selectivity at relatively high turnover rate. Starting from CO_2 derivatives [50] and multicomponent catalysts [46], gaseous CO_2 can now be converted to methanol on a single metal complex

with excellent efficiency [48, 49]. While most of the well-performing catalysts are based on noble metals, especially Ru, catalysts consisting of non-noble metals such as Co [51] and Mn [52] have also been reported recently.

On the other hand, CO_2 capture and sequestration (CCS) has become increasingly important due to the urgent need to lower the global CO_2 level [53, 54]. Coupling of CO_2 capture and its subsequent conversion to liquid fuels such as methanol in the so-called carbon capture and recycling (CCR) strategy would provide a one-pot scheme towards the production of renewable fuels directly from the captured CO_2, thus bypassing the energy penalty conventionally introduced from the desorption and compression process.

In this context, Olah and Prakash have demonstrated the possibility of capturing CO_2 directly from air and converting it to methanol on a robust Ru-based catalyst [55]. In their system, a short-chain polyamine, pentaethylenehexamine (PEHA), was used for CO_2 capture for its excellent solubility in the reaction solvent as compared to the conventional polyehtylenimine (PEI). Superbases such as DBU (1,8-diazabicycloundec-7-ene) and TMG (1,1,3,3-tetramethyl guanidine) were also tested as substituents to PEHA but showed very little methanol production. A Ru-Macho-BH pincer complex (Catalyst 1 or C-1, Fig. 4c) displayed the best performance, in which the –NH moiety was proven to be crucial and its substitution led to no alcohol formation.

Another advantage of their catalyst is its robustness, which can be seen from both its thermal stability and recyclability (Fig. 4a, b). As compared to other catalyst systems which would otherwise decompose if not heated via a "temperature ramp" strategy that involves a preheating step at lower temperatures [56], directly heating the reaction mixture with C-1 to the reaction temperature for prolonged time showed continuous formation of methanol. Recyclability test showed > 75% of the initial activity after five cycles. Further refinement of the reaction conditions led to an optimal methanol production with 5.1 mmol of PEHA, 20 µmol of C-1, and triglyme as the solvent. At 145 °C, a methanol yield

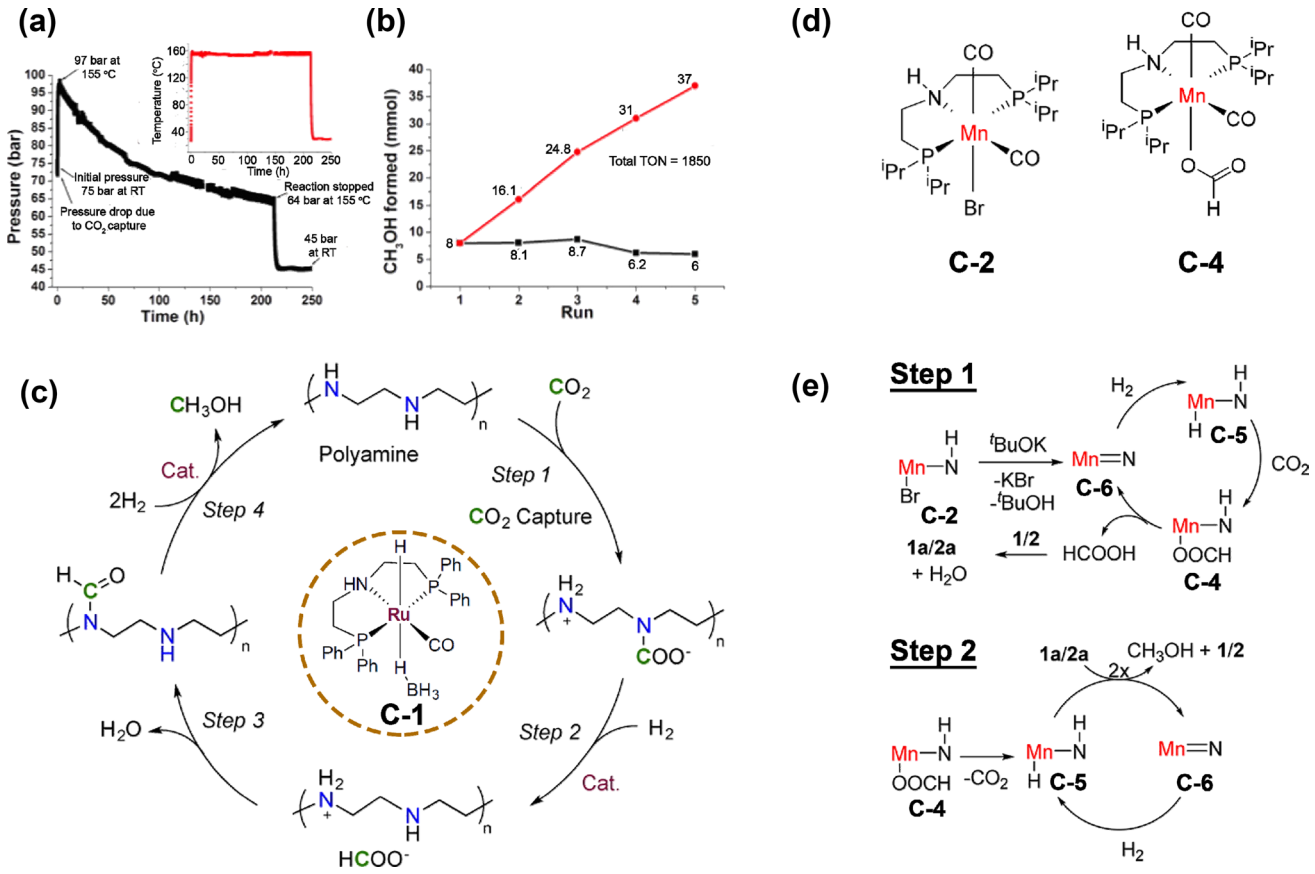

Fig. 4 **a** Pressure inside the reaction vessile as a function of reaction time. **b** CH_3OH formed in each run (black line) and cumulative CH_3OH production as a function of the number of runs (red line, t = 40 h for each run), as determined by ^1H NMR. Reaction conditions for (**a, b**): PEHA = 3.4 mmol, C-1 = 20 µmol, CO_2/H_2 (1/3) = 75 bar, T = 155 °C, and THF = 10 mL. **c** Proposed reaction mechanism with C-1. **d** Molecular structure of catalyst C-2 and key intermediate species C-4. **e** Proposed reaction mechanism with C-2. **a**–**c** Adapted with permission from reference [55]. Copyright 2016 American Chemical Society; **d, e** adapted with permission from reference [52]. Copyright 2017 American Chemical Society

as high as 65% was achieved with a 1:9 ratio of CO_2/H_2 at 75 bar and t = 200 h.

More importantly, when using air as the only source of CO_2, about 1.6 mmol of CO_2 could be captured per mmol of PEHA and a methanol yield of 79% could be achieved at 155 °C and t = 55 h. This demonstrates for the first time the feasibility of using CO_2 captured directly from air for the production of methanol.

In a later work, Prakash and co-workers demonstrated the possibility of using an inexpensive Mn(I) complex to catalyze the transformation of amine-captured CO_2 to methanol [52]. This is of particular interest since it offered a lower-cost and easier-obtainable alternative to the more widely used noble metal based catalysts.

A Mn-pincer complex (catalyst 2 or C-2, Fig. 4d) was firstly tested for its effectiveness in the N-formylation of amine with CO_2 and H_2, which is the first step of the sequential process. The results indicate that C-2 could satisfyingly reduce CO_2 to formamide with a yield up to 94% with *N*-methylbenzylamine after 24 h of reaction at 110 °C in THF. The subsequent reduction of the in situ formed formamide to CH_3OH with C-2 was carried out by subjecting the reaction mixture from the previous step to H_2, which was proven to be successful. CH_3OH yield up to 71% was obtained with a catalyst loading and H_2 pressure of 2 mol% and 80 bar, respectively, after 36 h of reaction at 150 °C. Mechanistic studies with ^1H and ^{31}P NMR revealed the formation of complex C-4 (Fig. 4d) during the initial N-formylation step, which then gets decarboxylated in the subsequent formamide reduction step at high H_2 pressure to form back active catalytic species C-5, which in turn reduces the in situ formed formamide (Fig. 4e). Further attempts towards one-step methanol synthesis in the presence of C-2 with low CO_2 and high H_2 pressure was unsatisfying with only traces of methanol formed. Exploration and optimization of the catalyst systems would need to be made as well as the refinement of the reaction process in order to tackle the problem.

2.3 Catalytic Conversion of Methane to Methanol

2.3.1 Direct Methane Oxidation to Methanol (DMTM)

Current technology for the conversion of methane to methanol includes the generation of syngas by reforming of methane followed by the hydrogenation of CO and CO_2, which is a two-step process. The formation of syngas by methane reforming proceeds at high temperatures and is therefore energy-intensive. On the contrary, direct route to partially oxidize methane to methanol in principle can proceed more efficiently and cost-effectively at lower temperatures [57]. There has been substantial efforts to develop direct and selective methane oxidation which possesses great potential but remains as a challenge.

Various heterogeneous catalysts have been tested in DMTM and most of them showed formaldehyde as the major product which is further oxidized from methanol (i.e. magnesium-, molybdenium-, and vanadium-based catalysts) [58–63]. Precious metal NPs usually result in total oxidation to CO_2 as methane oxygenates are typically more reactive than methane and therefore hard to be preserved [64–66]. Despite substantial efforts, it was suffered by low selectivity to methanol until new active sites are found in Fe–ZSM-5 and Cu–ZSM-5 which resemble the active site of soluble methane monooxygenase (sMMO) and particulate methane monooxygenase (pMMO), respectively [67, 68]. The main difference between the two catalysts is the activation process, where the active site in Fe–ZSM-5 is only formed with N_2O through heating while Cu–ZSM-5 is capable of being activated by O_2 or N_2O at lower temperatures, which is more efficient.

Groothaert et al. tried Cu–ZSM-5 (Na-form) for methane oxidation and found that it produces methanol as the sole product [68]. They used a combined GC-UV–vis setup to study the interaction of methane with O_2-activated Cu–ZSM-5 (Si/Al = 12 and Cu/Al = 0.58) at 723 K. An absorption band at 22,700 cm^{-1} was observed in the UV–vis spectrum, which disappeared within 3 min after methane was introduced at 448 K (Fig. 5a). This result indicates that copper-oxo species related with the absorption band at 22,700 cm^{-1} is the active site for methane oxidation. Despite this observation, they could not detect any product in GC analysis and instead used the extraction method with a 1/1 ratio of water/acetonitrile mixture which gave 8.2 µmol of methanol per gram of Cu–ZSM-5. Later, they defined the active site in Cu–ZSM-5 to be the bent mono-(µ-oxo)dicupric site $[Cu(\mu\text{-}O)Cu]^{2+}$ ($\angle CuOCu = 139°$) as evidenced by resonance Raman (rR) coupled to normal coordinate (NCA) and density functional theory (DFT) calculation (Fig. 5b). The 22,700 cm^{-1} band in UV-vis spectrum is attributed to the bridging oxo ligand to Cu charge transfer. A precursor of mono-(µ-oxo)dicupric site $[Cu(\mu\text{-}O)Cu]^{2+}$ was discovered with characteristic absorption band at 29,000 cm^{-1}, which was attributed to $\mu\text{-}(\eta^2\text{:}\eta^2)$ peroxo dicopper(II) species $[Cu_2(O_2)]^{2+}$ [69]. Two additional electrons are provided by spectator Cu^+ ions in the neighboring ion-exchanged sites.

This finding motivated further research on Cu-based zeolites with various topologies. It is found that only Cu exchanged zeolites ZSM-5 and MOR are capable of converting methane to methanol at low temperature (150 °C) whereas Cu-FER and Cu-BEA require higher temperature (200 °C) to be active. In addition, Cu-MOR was shown to have higher activity at 200 °C, which implies that it has different active copper-oxo species from Cu–ZSM-5 [70].

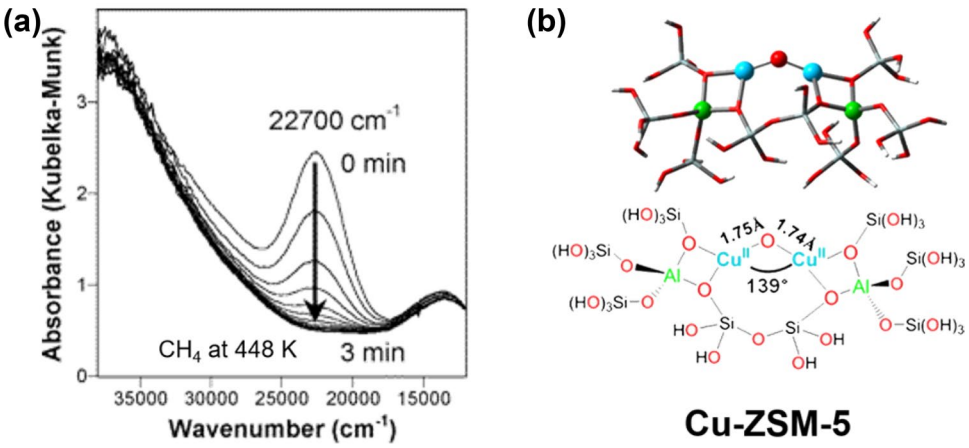

Fig. 5 **a** Fiber-optic UV–vis spectra of O_2-activated Cu–ZSM-5 (Si/Al = 12 and Cu/Al = 0.58) during reaction with CH_4 (5% in N_2, 25 mL min^{-1}) at 448 K. **b** Proposed active site as the bent mono-(μ-oxo) dicupric site $[Cu(\mu\text{-}O)Cu]^{2+}$ in Cu–ZSM-5. **a** Adapted with permission from reference [68]. Copyright 2005 American Chemical Society; **b** adapted with permission from reference [69]. Copyright 2009 National Academy of Sciences

Single-site trinuclear copper oxygen clusters $[Cu_3(\mu\text{-}O)_3]^{2+}$ in H-MOR (Fig. 6a) was proposed later as the active site which are anchored to two framework Al atoms located at the pore mouth of the 8-MR side pockets [71]. This structure is optimized by O_2 and N_2O at 450 and 600 °C, respectively, where Cu-MOR activated by N_2O at 600 °C produces 97 μmol of methanol per gram of catalyst, which is 1.5 times higher than Cu-MOR activated by O_2 at 450 °C (Fig. 6b) [72]. The difference between N_2O and O_2 activation is attributed to the different values of negative change in entropy during the formation of the active copper species $[Cu_3(\mu\text{-}O)_3]^{2+}$. Not only in the mordenite zeolite, the presence of trinuclear copper oxygen clusters $[Cu_3(\mu\text{-}O)_3]^{2+}$ in ZSM-5 was also suggested by DFT calculation as the most stable extra-framework Cu species in Cu/ZSM-5 activated by calcination, whereas the formation of the binuclear complexes $[Cu(\mu\text{-}O)Cu]^{2+}$ is favored under O_2-poor atmosphere [73]. Given the high potential resemblance of Cu-based zeolite to pMMO, further researches on the copper-oxo species are expected.

Compared to the advancements that have been made in the development of heterogeneous catalysts, there has been less progress in process development. Currently, for the DMTM process on heterogeneous Cu–zeolites, sequential treatment consisting of three steps is required. The first step is the activation by N_2O/O_2 which helps to form the active copper oxo species (over 400 °C). The second step is the so-called adsorption of methane (up to about 200 °C), which is then followed by extraction using H_2O (up to about 200 °C). To recycle the catalyst after the three-step reaction, thermal treatment of the catalyst to desorb water molecules is essential (over 400 °C). As the optimal temperature is different for each step, co-feeding of oxidant, methane, and steam in a single step is hindered, yet there are still some attempts to do so. On Cu–ZSM-5 activated at 450 °C under flowing O_2, Román-Leshkov and co-workers observed steady state methanol production rates of 0.88 ± 0.02 μmol h^{-1} $g_{cat}{}^{-1}$ and 1.81 ± 0.01 μmol h^{-1} $g_{cat}{}^{-1}$ for Cu–Na–ZSM-5 (Cu/Al = 0.37, Na/Al = 0.26) and Cu–H–ZSM-5 (Cu/Al = 0.31), respectively, at 210 °C by flowing a gas mixture of 98.1 kPa

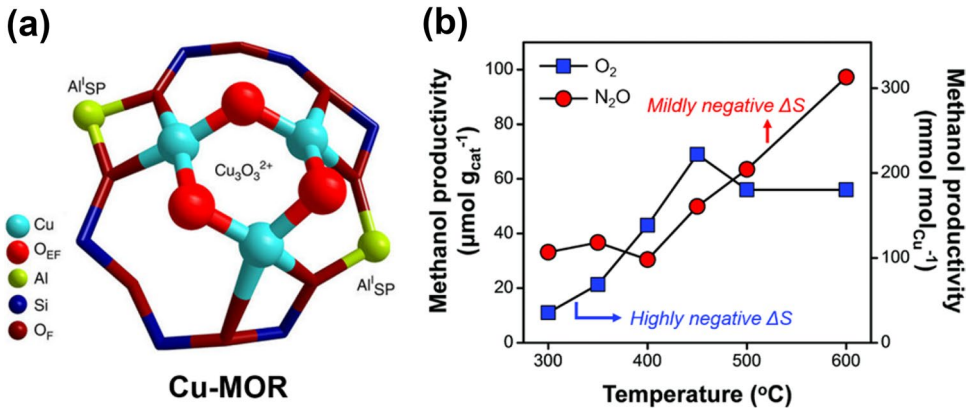

Fig. 6 **a** Proposed location of trinuclear copper oxygen clusters $[Cu_3(\mu\text{-}O)_3]^{2+}$ in H-mordenite. **b** Methanol production over Cu-MOR (Si/Al = 20, Cu/Al = 0.4) activated by O_2 (blue) and N_2O (red) at different activation temperatures followed by reaction with methane at 150 °C and extraction with steam at 135 °C. **a** Adapted with permission from reference [71]. Copyright 2015 Springer Nature; **b** adapted with permission from reference [72]. Copyright 2017 Royal Society of Chemistry

of methane, 3.2 kPa of H_2O, and 0.0025 kPa of O_2 [74]. Besides using the temperature swing that was described above, it is also possible to enable methanol production with elevated pressure of methane during the reaction. This can be understood by a kinetic study on Cu–Na–ZSM-5 (Cu/Al = 0.37, Na/Al = 0.26) at 210 °C which shows first, half, and zero order dependencies with respect to methane, H_2O, and O_2, respectively [74]. Bokhoven and co-workers carried out activation and methane reaction isothermally at 200 °C and 1 bar of O_2 with a 13 h activation period on Cu-MOR (Si/Al = 6, 4.7 wt% Cu). The methanol yield was found to gradually increase from 0.3 to 56.2 μmol g^{-1} as the methane pressure increased from 50 mbar to 37 bar [75]. Recently, the use of H_2O which plays a key role in both methanol extraction and catalyst regeneration is reported, however, it cannot escape from utilizing the temperature swing [76]. Therefore, besides the development of novel catalyst systems, process conditions are equally important and need to be studied carefully in order to implement the DMTM process.

2.3.2 The 'Metgas' Approach: Bi-reforming of Methane

Although it might seem to be less elegant as compared to the direct route, indirect methanol production from CH_4 via syngas dates back long and has been extensively studied. Most industrial practices rely on this technique, which have been fulfilling the majority of the methanol demand worldwide.

Syngas can be produced in various ways, with steam reforming (Eq. 6) and dry reforming (Eq. 7) of CH_4 being the most important ones. However, neither of them could deliver syngas with the correct ratio of H_2 to CO without purification and adjustment. In addition, coke formation would inevitably hurt the performance of the catalyst, especially in the case of the dry reforming process [77]. To address these issues, Olah and co-workers combined the steam reforming and dry reforming of methane in a single step called bi-reforming (Eq. 8) to deliver a syngas of exactly a 2/1 H_2/CO ratio (named 'metgas') [78–80], which is just right for the methanol production. Besides, bi-reforming also benefits from its resistance to coke formation due to the presence of steam [81], tolerance for various CH_4 sources with different levels of CO_2 impurities as the H_2O/CO_2 ratio is easily controllable, and ability to operate at high pressures which is convenient for downstream processes, making it ideal for feeding methanol synthesis.

$$\text{Steam reforming} \quad 2CH_4 + 2H_2O \rightarrow 2CO + 6H_2 \quad \Delta H_{298\,K} = +98.6\ \text{kcal/mol} \tag{6}$$

$$\text{Dry reforming} \quad CH_4 + CO_2 \rightarrow 2CO + 2H_2 \quad \Delta H_{298\,K} = +59.1\ \text{kcal/mol} \tag{7}$$

$$\text{Bi-reforming} \quad 3CH_4 + 2H_2O + CO_2 \rightarrow 4CO + 8H_2 \quad \Delta H_{298\,K} = +157.7\ \text{kcal/mol} \tag{8}$$

Bi-reforming is preferentially carried out at 800–950 °C and 5–40 atm with a feed composition of CH_4, steam, and CO_2 in a ratio of 3/2/1. In their work, various metals such as V, Ti, Ga, Ca, Mo, Bi, Fe, Co, Nb, Zr, La, and Sn along with their corresponding oxides were supported on different supports including alumina and silica and tested for their activity in bi-reforming. Among the catalysts tested, NiO deposited on MgO synthesized via a simple wet impregnation method was proven to be ideal for the process. The NiO content in the catalyst was varied in the range of 5–35% and no major effect was observed on its catalytic performance.

In a typical experiment, catalysts are first activated with a 1/1 ratio of H_2/N_2 at 850 °C for 3 h. An excess of CO_2 and H_2O was employed to partially compensate for the loss in CH_4 conversion at elevated pressures, resulting in a real gas feed composition of 3/2.4/1.2 for $CH_4/H_2O/CO_2$. At 830 °C, 7 bar, and a total flow rate of 100 mL/min, the catalyst could deliver a stable CH_4 and CO_2 conversion of 71 and 62%, respectively, as well as a steady H_2/CO ratio very close to two with near 100% selectivity for a prolonged time of 320 h (Fig. 7a, b). Raising the reaction temperature from 830 to 910 °C or pressure from 7 to 42 bar resulted in a 21% increase or a 41% decrease in CH_4 conversion, respectively, while the variation in the H_2/CO ratio was minimal (within 2%) (Fig. 7c, d). To further demonstrate its capability for practical application, bi-reforming was carried out with natural gas. The results are encouraging, where all the long-chain hydrocarbons in the natural gas were successfully converted to metgas and had no obvious negative impact on the activity and stability of the catalyst. The H_2/CO ratio obtained (1.9 at 7 bar) was slightly lower than the target value but could be easily adjusted by simply increasing the amount of steam to account for the higher alkanes, according to Eq. 9. This demonstrates the adaptability of the technique, which is essential to accommodate natural gas sources with various compositions and CO_2 content.

$$3C_nH_{2n+2} + (3n-1)H_2O + CO_2 \rightarrow (3n+1)CO + (6n+2)H_2 \tag{9}$$

To push things one-step further, Olah and co-workers developed the so-called oxidative bi-reforming, where the energy and 2/1 ratio of H_2O/CO_2 mixture needed for the endothermic bi-reforming process are supplied by the complete combustion of CH_4. A scheme of its operation is shown in Fig. 7e. By generating energy and H_2O/CO_2 mixture in situ, oxidative bi-reforming is essentially a self-sufficient process. When combined with the subsequent methanol synthesis, a complete exclusive oxygenation of CH_4 to methanol could be achieved.

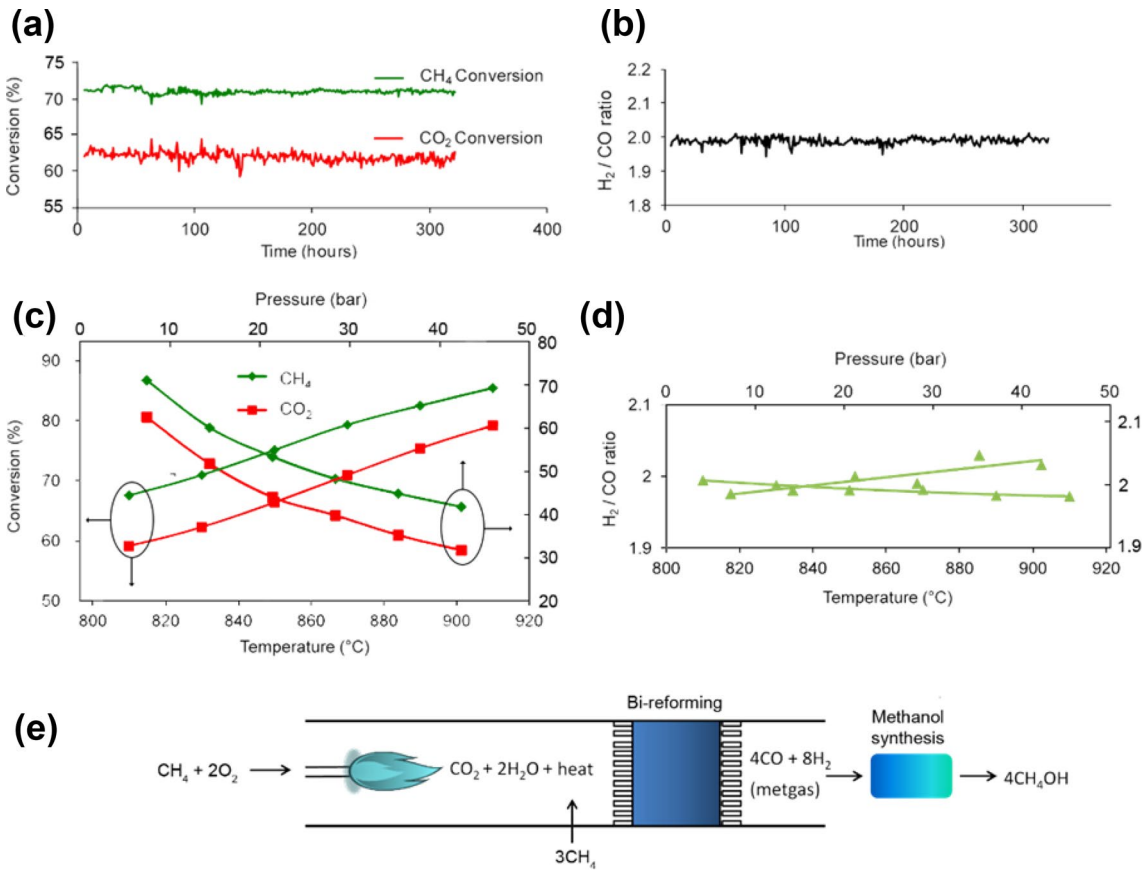

Fig. 7 **a, b** Reaction conversion and H_2/CO ratio as a function of time on stream. **c, d** Reaction conversion and H_2/CO ratio as a function of reaction temperature and pressure. **e** Operating scheme of oxidative bi-reforming. Adapted with permission from reference [77]. Copyright 2015, American Chemical Society

As compared to the autothermal reforming (ATR) process where the endothermic methane steam reforming is combined with its partial oxidation in order to achieve energy-neutral [82], oxidative bi-reforming outperforms by its simplicity and almost zero generation of by-products, while the ATR process involves costly multi-step separation and adjustment and produces large amount of CO_2 necessitating its sequestering or venting into the atmosphere [83, 84]. On the other hand, challenges such as safety concerns related with the CH_4/O_2 mixture in the combustion step and catalyst resistance to high temperature and steam environment do exist and require further research.

Not only for methanol synthesis, bi-reforming and oxidative bi-reforming also have powerful potential as alternatives to provide feed for Fischer–Tropsch synthesis in gas-to-liquids (GTL) process, especially for the low-temperature Fischer–Tropsch reaction where cobalt-based catalysts are used due to their low activity towards WGS reaction.

With the world reserve still expanding thanks to the discovery of new types of natural gas resources and the advancement of latest drilling technologies, bi-reforming of CH_4 and the subsequent methanol synthesis through metgas appear to be particularly promising in providing renewable synthetic fuels, which would gradually take over the already depleting petroleum oil to power up our everyday activities in the future [84]. In addition, utilization of CO_2 captured and recycled from power plant exhaust and other human activities would help mitigate the greenhouse effect and alleviate global climate change, making the process truly sustainable. With advanced research underway, more comprehensive understanding of this technology will be acquired, paving the road towards its commercialization [81].

3 Conclusions and Outlook

With the gradual depletion of petroleum oil and the awareness to protect earth's ecosystem, we are now more aggressively pursuing the recyclability of carbon and the development of new types of energy sources that are cleaner and truly sustainable than ever before. Prof. Olah and his research team have dedicated years of their research

focusing on the development of methanol economy, which not only provides an alternative energy source and chemical building block, but also promotes the capture and recycling of CO_2, thus playing an important role in minimizing the harmful environmental effect of carbon emission and achieving true sustainability.

Current technology permits sustained production of methanol from natural gas, which would likely last well into the next century thanks to the discovery of unconventional resources such as shale gas and methane hydrate [35]. However, efforts still need to be made towards a higher efficiency of the process. Advanced technologies such as bi-reforming are to be tested in practical settings and single-step oxygenation of CH_4 to methanol would be more attractive if we can push the yield to meet the industrial requirement.

CO_2 from plant exhaust and other recycled sources is ideal for the production of renewable methanol through its hydrogenation. This approach has been practiced and commercialized heterogeneously since 2012 at the "George Olah Renewable Plant" in Iceland with Cu/ZnO based catalyst [35]. As our understanding about the catalyst system deepens [22, 28, 43, 85] and the technology on clean H_2 generation and CO_2 capture advances, larger scale implementation can be expected. At the same time, novel catalysts are also being continuously developed to offer outstanding performance, yet their potential in practical settings takes time to be evaluated.

Research concerning the homogeneous CO_2 hydrogenation to methanol has just started to bloom. Its capability of operating at milder conditions with superb selectivity plus the flexibility to tailor the performance of the catalyst makes the homogeneous route rather attractive. However, as appealing as it is, there are mountains to climb before it can be practically viable. Reaction rate needs to be further improved in order to operate in a continuous mode. Non-noble metal based catalysts are to be developed to cut the requirement for noble metals. In addition, comprehensive mechanistic study needs to be carried out to serve as guidance for catalyst optimization.

In addition, heterogenized homogeneous catalysts might bring in some unique insights and open up more possibilities [86]. By fabricating single molecularly defined metal complexes or metal clusters on heterogeneous supports through techniques such as surface organometallic and coordination chemistry [87–89], it would give more handles for tuning the catalytic performance and improve the recyclability and regeneration of the catalyst at the same time, which are favored in practical applications.

Acknowledgements This work was supported by the Director, Office of Science, Office of Basic Energy Sciences, Division of Chemical Sciences, Geological, and Biosciences, U.S. Department of Energy, under Contract DEAC02-05CH11231.

References

1. Olah GA (2005) Angew Chem Int Ed 55:2636–2639
2. Olah GA (2013) Angew Chem Int Ed 52:104–107
3. Goeppert A, Olah GA, Prakash GKS (2018) Toward a sustainable carbon cycle: the methanol economy. Elsevier Inc, Amsterdam
4. Anderson JE, Kramer U, Mueller SA, Wallington TJ (2010) Energy Fuels 24:6576–6585
5. Chen G, Shen Y, Zhang Q, Yao M, Zheng Z, Liu H (2013) Energy 54:333–342
6. Abu-Zaid M, Badran O, Yamin J (2004) Energy Fuels 18:312–315
7. Moffat A (1991) Science 251:514–515
8. Kumar P, Dutta K, Das S, Kundu PP (2014) Int J Energy Res 38:1367–1390
9. Ahmed M, Dincer I (2011) Int J Energy Res 35:1213–1228
10. Aricò AS, Srinivasan S, Antonucci V (2001) Fuel Cells 1:133–161
11. McGrath KM, Prakash GKS, Olah GA (2004) J Ind Eng Chem 10:1063–1080
12. Radenahmad N, Ahmed A, Iskandar PI, Rahman SMH, Eriksson S, Azad AK (2016) Renew Sustain Energy Rev 57:1347–1358
13. Ilias S, Bhan A (2013) ACS Catal 3:18–31
14. Tian P, Wei Y, Ye M, Liu Z (2015) ACS Catal 5:1922–1938
15. Olsbye U, Svelle S, Bjørgen M, Beato P, Janssens TVW, Joensen F, Bordiga S, Lillerud KP (2012) Angew Chem Int Ed 51:5810–5831
16. Sheldon D (2017) Johnson Matthey Technol Rev 61:172–182
17. Wender I (1996) Fuel Process Technol 48:189–297
18. Aresta M, Dibenedetto A (2007) Dalton Trans 0:2975–2992
19. Chanchlani KG, Hudgins RR, Silveston PL (1992) J Catal 136:59–75
20. Waugh KC (1992) Catal Today 15:51–75
21. Chinchen GC, Denny PJ, Parker DG, Spencer MS, Whan DA (1987) Appl Catal 30:333–338
22. Kuld S, Thorhauge M, Falsig H, Elkjær CF, Helveg S, Chorkendorff I, Sehested J (2016) Science 352:969–974
23. Samson K, Sliwa M, Socha RP, Góra-Marek K, Mucha D, Rutkowska-Zbik D, Paul JF, Ruggiero-Mikoajczyk M, Grabowski R, Soczyński J (2014) ACS Catal 4:3730–3741
24. Baltes C, Vukojević S, Schüth F (2008) J Catal 258:334–344
25. Arena F, Barbera K, Italiano G, Bonura G, Spadaro L, Frusteri F (2007) J Catal 249:185–194
26. Kurtz M, Bauer N, Büscher C, Wilmer H, Hinrichsen O, Becker R, Rabe S, Merz K, Driess M, Fischer R, Muhler M (2004) Catal Lett 92:49–52
27. Becker R, Parala H, Hipler F, Tkachenko OP, Klementiev KV, Grünert W, Wilmer H, Hinrichsen O, Muhler M, Birkner A, Wöll C, Schäfer S, Fischer RA (2004) Angew Chem Int Ed 43:2839–2842
28. Kattel S, Ramírez PJ, Chen JG, Rodriguez JA, Liu P (2017) Science 355:1296–1299
29. Labinger JA, Bercaw JE (2002) Nature 417:507–514
30. Arndtsen BA, Bergman RG, Mobley TA, Peterson TH (1995) Acc Chem Res 28:154–162
31. Barton DHR (1990) Aldrichimica Acta 23:1990
32. Kwon Y, Kim TY, Kwon G, Yi J, Lee H (2017) J Am Chem Soc 139:17694–17699
33. Ikuno T, Zheng J, Vjunov A, Sanchez-Sanchez M, Ortuño MA, Pahls DR, Fulton JL, Camaioni DM, Li Z, Ray D, Mehdi BL, Browning ND, Farha OK, Hupp JT, Cramer CJ, Gagliardi L, Lercher JA (2017) J Am Chem Soc 139:10294–10301

34. Rahim A, Hasbi M, Forde MM, Jenkins RL, Hammond C, He Q, Dimitratos N, Lopez-Sanchez JA, Carley AF, Taylor SH, Willock DJ, Murphy DM, Kiely CJ, Hutchings GJ (2013) Angew Chem 125:1318–1322
35. Goeppert A, Czaun M, Jones J-P, Prakash GKS, Olah GA (2014) Chem Soc Rev 43:7995–8048
36. http://carbonrecycling.is. Accessed 15 Jan 2018
37. Li CS, Melaet G, Ralston WT, An K, Brooks C, Ye Y, Liu YS, Zhu J, Guo J, Alayoglu S, Somorjai GA (2015) Nat Commun 6:6538. https://doi.org/10.1038/ncomms7538
38. Martin O, Martín AJ, Mondelli C, Mitchell S, Segawa TF, Hauert R, Drouilly C, Curulla-Ferré D, Pérez-Ramírez J (2016) Angew Chem Int Ed 55:6261–6265
39. Wang J, Li G, Li Z, Tang C, Feng Z, An H, Liu H, Liu T, Li C (2017) Sci Adv 3:e1701290
40. Kattel S, Liu P, Chen JG (2017) J Am Chem Soc 139:9739–9754
41. Rodriguez JA, Liu P, Stacchiola DJ, Senanayake SD, White MG, Chen JG (2015) ACS Catal 5:6696–6706
42. An K, Alayoglu S, Musselwhite N, Plamthottam S, Melaet G, Lindeman AE, Somorjai GA (2013) J Am Chem Soc 135:16689–16696
43. Behrens M, Studt F, Kasatkin I, Kühl S, Hävecker M, Abild-pedersen F, Zander S, Girgsdies F, Kurr P, Kniep B, Tovar M, Fischer RW, Nørskov JK, Schlögl R (2012) Science 336:893–897
44. Rungtaweevoranit B, Baek J, Araujo JR, Archanjo BS, Choi KM, Yaghi OM, Somorjai GA (2016) Nano Lett 16:7645–7649
45. Long J, Wang S, Ding Z, Wang S, Zhou Y, Huang L, Wang X (2012) Chem Commun 48:11656–11658
46. Huff CA, Sanford MS (2011) J Am Chem Soc 133:18122–18125
47. Wesselbaum S, Vom Stein T, Klankermayer J, Leitner W (2012) Angew Chem Int Ed 51:7499–7502
48. Alberico E, Nielsen M (2015) Chem Commun 51:6714–6725
49. Li Y-N, Ma R, He L-N, Diao Z-F (2014) Catal Sci Technol 4:1498–1512
50. Balaraman E, Gunanathan C, Zhang J, Shimon LJW, Milstein D (2011) Nat Chem 3:609–614
51. Schneidewind J, Adam R, Baumann W, Jackstell R, Beller M (2017) Angew Chem Int Ed 56:1890–1893
52. Kar S, Goeppert A, Kothandaraman J, Prakash GKS (2017) ACS Catal 7:6347–6351
53. Breeze P (2009) Science 325:1647–1652
54. Chu S (2009) Science 325:1599
55. Kothandaraman J, Goeppert A, Czaun M, Olah GA, Prakash GKS (2016) J Am Chem Soc 138:778–781
56. Rezayee NM, Huff CA, Sanford MS (2015) J Am Chem Soc 137:1028–1031
57. Ravi M, Ranocchiari M, Bokhoven JA, Van (2017) Angew Chem Int Ed 56:16464–16483
58. Nguyen LD, Loridant S, Launay H, Pigamo A, Dubois JL, Millet JMM (2006) J Catal 237:38–48
59. Zhen KJ, Khan MM, Mak CH, Lewis KB, Somorjai GA (1985) J Catal 94:501–507
60. Taylor SH, Hargreaves JSJ, Hutchings GJ, Joyner RW, Lembacher CW (1998) Catal Today 42:217–224
61. Sugino T, Kido A, Azuma N, Ueno A, Udagawa Y (2000) J Catal 190:118–127
62. Hargreaves JSJ, Hutchings GJ, Joyner RW (1990) Nature 348:428–429
63. Fornés V, López C, López HH, Martinez A (2003) Appl Catal A 249:345–354
64. Briot P, Primet M (1991) Appl Catal 68:301–314
65. Hicks RF, Qi H, Young ML, Lee RG (1990) J Catal 122:280–294
66. Rotko M, Machocki A, Słowik G (2017) Catal Lett 147:1783–1791
67. Sobolev VI, Dubkov KA, Panna OV, Panov GI (1995) Catal Today 24:251–252
68. Groothaert MH, Smeets PJ, Sels BF, Jacobs PA, Schoonheydt RA (2005) J Am Chem Soc 127:1394–1395
69. Woertink JS, Smeets PJ, Groothaert MH, Vance MA, Sels BF, Schoonheydt RA, Solomon EI (2009) Proc Natl Acad Sci 106:18908–18913
70. Smeets PJ, Groothaert MH, Schoonheydt RA (2005) Catal Today 110:303–309
71. Grundner S, Markovits MAC, Li G, Tromp M, Pidko EA, Hensen EJM, Jentys A, Sanchez-Sanchez M, Lercher JA (2015) Nat Commun 6:7546. https://doi.org/10.1038/ncomms8546
72. Kim Y, Kim TY, Lee H, Yi J (2017) Chem Commun 53:4116–4119
73. Li G, Vassilev P, Sanchez-Sanchez M, Lercher JA, Hensen EJM, Pidko EA (2016) J Catal 338:305–312
74. Narsimhan K, Iyoki K, Dinh K, Román-Leshkov Y (2016) ACS Cent Sci 2:424–429
75. Tomkins P, Mansouri A, Bozbag SE, Krumeich F, Park MB, Alayon EMC, Ranocchiari M, Vanbokhoven JA (2016) Angew Chem 128:5557–5561
76. Sushkevich VL, Palagin D, Ranocchiari M, Bokhoven JA van (2017) Science 356:523–527
77. Muraza O, Galadima A (2015) Int J Energy Res 39:1196–1216
78. Olah GA, Goeppert A, Czaun M, Prakash GKS (2013) J Am Chem Soc 135:648–650
79. Olah GA, Prakash GKS, Goeppert A, Czaun M, Mathew T (2013) J Am Chem Soc 135:10030–10031
80. Olah GA, Goeppert A, Czaun M, Mathew T, May RB, Prakash GKS (2015) J Am Chem Soc 137:8720–8729
81. Kumar N, Shojaee M, Spivey JJ (2015) Curr Opin Chem Eng 9:8–15
82. Sousa-Aguiar EF, Noronha FB, Faro A Jr (2011) Catal Sci Technol 1:698–713
83. Olah GA, Prakash GKS (2015) US Patent: 8,980,961
84. Olah GA (2013) Catal Lett 143:983–987
85. Studt F, Behrens M, Kunkes EL, Thomas N, Zander S, Tarasov A, Schumann J, Frei E, Varley JB, Abild-Pedersen F, Norskov JK, Schlogl R (2015) ChemCatChem 7:1105–1111
86. Ye R, Zhukhovitskiy AV, Deraedt CV, Toste FD, Somorjai GA (2017) Acc Chem Res 50:1894–1901
87. Guzman J, Gates BC (2003) Dalton Trans 0:3303–3318
88. Copéret C, Comas-Vives A, Conley MP, Estes DP, Fedorov A, Mougel V, Nagae H, Núnez-Zarur F, Zhizhko PA (2016) Chem Rev 116:323–421
89. Copéret C, Chabanas M, Saint-Arroman RP, Basset J-M (2003) Angew Chem Int Ed 42:156–181